Supporting Information

Semi-Fluorinated Polymer Membranes by Ring-Opening Metathesis Polymerization during Spin Coating

Tyler D. Oddo[1], Arun Srikanth[2], Zane J. Parkerson[1], Matthew P. Vasuta[3], Co D. Quach[1], Clare McCabe,[2] and G. Kane Jennings[1,2]

[1]Department of Chemical and Biomolecular Engineering, Vanderbilt University, Nashville, TN 37235, USA

[2]Physical Sciences and Engineering, Heriot-Watt University, Edinburgh, UK

[3]Interdisciplinary Materials Science Program, Vanderbilt University, Nashville, TN 37235, USA

A. Catalyst Spin Speed Testing:

To determine the optimal spin speed for catalyst deposition during scROMP, multiple pNBF8 membranes (36 cm^2) were made under the same conditions except for varying the spin speed of catalyst deposition. Four samples were prepared at catalyst deposition spin speeds of 1000, 2000, 2500, and 3000 RPM. Digital photographs of these membranes are displayed in **Figure A1**. The green/brown regions in the images are parts of the surface that have been stained from the catalyst solution while white regions are the native color of the PAN support. This study indicates that the 1000 RPM spin speed is too low to provide uniform coverage of the surface, evidenced by the many gaps of white space near the edges of the support (**Figure A1a**). At 3000 RPM (**Figure A1d**), the corners of the support are slightly exposed, indicating that this speed is too fast, and the centrifugal forces produced at this speed remove the solution too quickly to allow appropriate coverage. At 2000 and 2500 RPM (**Figures A1b and A1c**, respectively), the films don't show any visible signs of non-uniform coverage. ATR-FTIR spectroscopy was performed

to determine if the corners of these membranes were appropriately covered with polymer (**Figure A2**). The spectra confirm the uniformity of the polymer film across the surface at both speeds, so a catalyst spin speed of 2000 or 2500 RPM was deemed acceptable. However, the 2000 RPM spectrum showed greater agreement across different regions of the film, so it was the spin speed chosen for this study. The monomer spin speed was typically 3000 RPM for NB and NBFn because these solutions were more viscous and required a higher spin speed to generate the same uniformity.

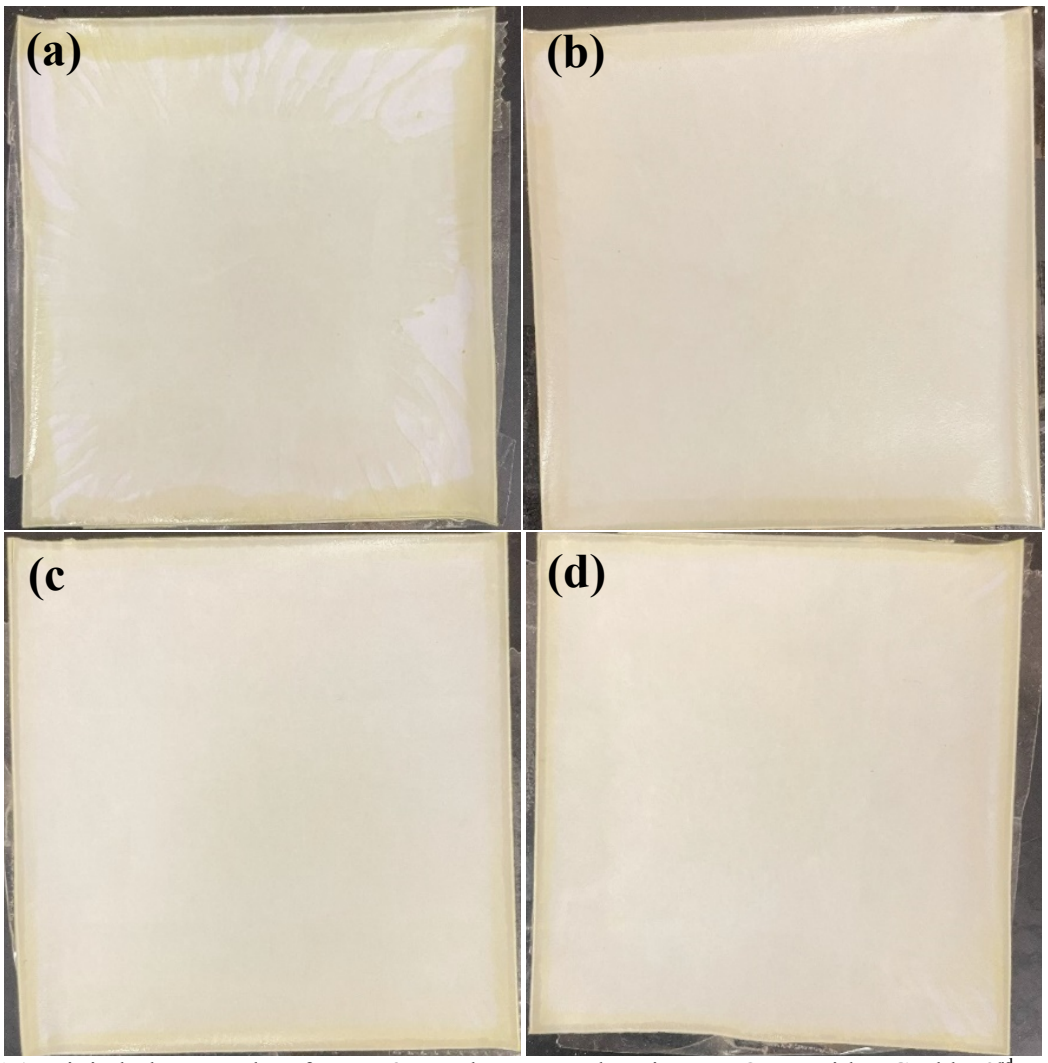

Figure A1: Digital photographs of pNBF8 membranes made using scROMP with a Grubbs 3rd generation catalyst deposition at a spin speed of (a) 1000, (b) 2000, (c) 2500, and (d) 3000 RPM. The results indicate that the spin speed for catalyst deposition should be between 2000 and 2500 RPM.

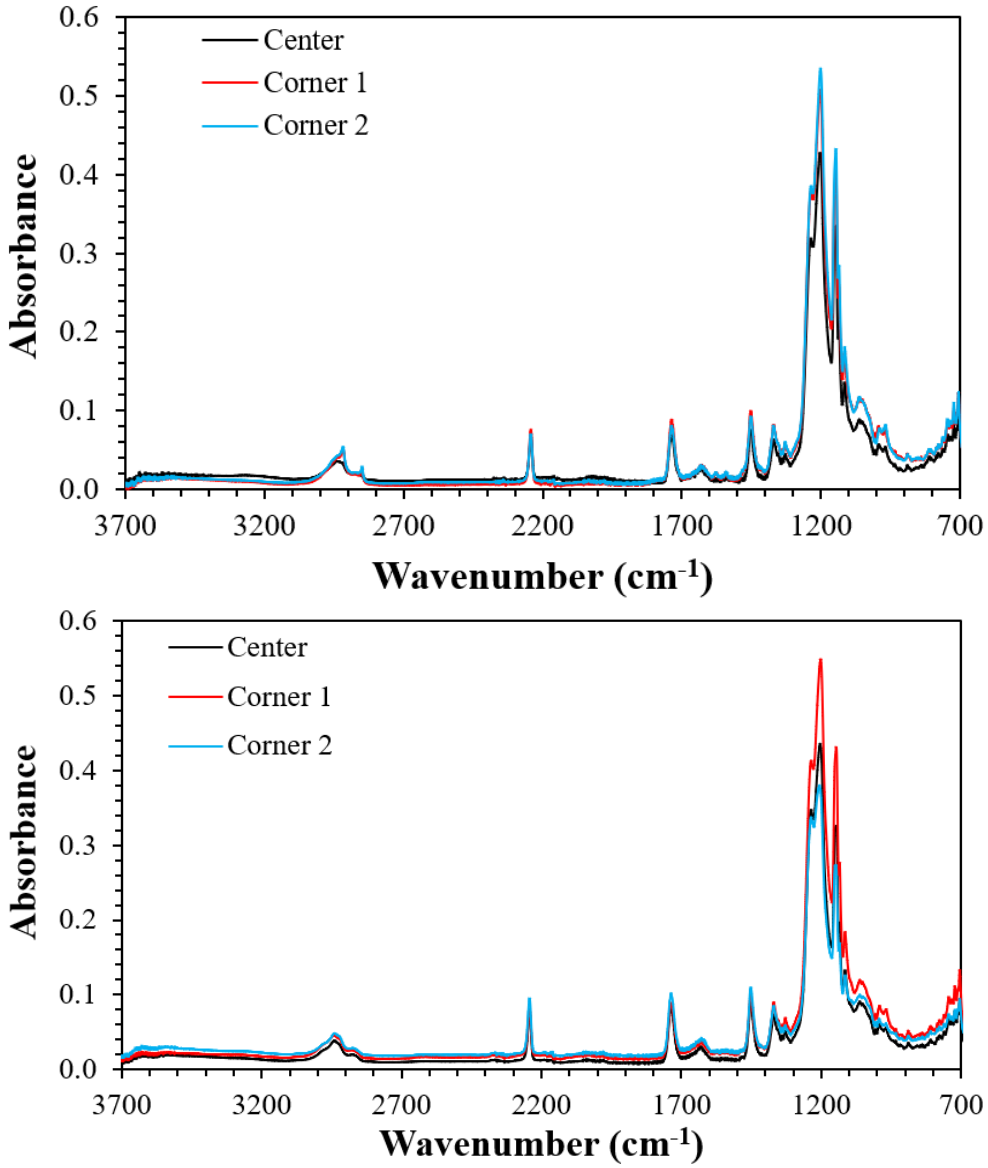

Figure A2: ATR-FTIR spectra of film b (top) and film c (bottom) from Figure A1. Corners 1 and 2 were on opposite diagonals from each other on a film. Film b shows greater uniformity of surface coverage than film c does, so a catalyst spin speed of 2000 RPM was deemed optimal.

B. Bondi Fractional Free Volume Calculation:

An estimate of fractional free volume (FFV) can be obtained using a group contribution method first developed by Bondi [1] and later expanded by Park and Paul [2]. This method describes the fractional free volume using the following equations

$$FFV = \frac{V_{sp} - 1.3V_w}{V_{sp}} \quad \text{(B1)}$$

$$V_w = \sum N_k * V_{w,k} \quad \text{(B2)}$$

$$V_{sp} = \sum N_k * \beta_k * V_{w,k} \quad \text{(B3)}$$

where V_w is the van der Waals volume, V_{sp} is the specific volume, FFV is the fractional free volume, β is a weighting factor relating van der Waals volume to specific volume, and N_k is the number of appearances of functional group k. **Table B1** summarizes the pertinent parameters of the functional groups in the pNBFn system.

Table B1: Summary of the van der Waals volume (V_w) and the scaling factor relating van der Waals volume to specific volume (β) for functional groups pertinent to this study.

Group Contribution	$\boldsymbol{V_w}$ $(\frac{cm^3}{mol})$	$\boldsymbol{\beta}$	**Source**
$-CF_3$	21.3	1.66	[2]
Decrement per cyclohexyl or cyclopentyl ring	-1.14	N/A	[1]
$-CH_2-$	10.23	1.33	[1,2]
$-CH_3$	13.67	1.38	[1,2]
$-CH$	6.78	1.30	[1,2]
$-CF_2-$	15.94	1.60	See text
$=CH$	8.47	1.799*	[1]

*The β value for $=CH-$ was estimated by calculating the free volume of polybutadiene and ensuring it matched values found in literature [3]

Two of the values represented in **Table B1** were not in the original manuscripts of Bondi or Park and Paul: the contribution of a $-CF_2-$ group and the β value of a $=CH-$ group. Since these functional groups,

especially a -CF_2-, are an integral part of the calculation, estimates were made to obtain reasonable values for the parameters. The -CF_2- data was calculated assuming the trend between CH_2 and CH_3 groups observed with the hydrocarbon data would follow for the fluorocarbon data. This allowed for the -CF_2- parameters to be calculated as follows:

$$V_{w,CF2} = \frac{V_{w,CH2}}{V_{w,CH3}} * V_{w,CF3} = \frac{10.23}{13.67} * 21.3 = 15.94 \quad \text{(B4)}$$

$$\beta_{CF2} = \frac{\beta_{w,CH2}}{\beta_{w,CH3}} * \beta_{w,CF3} = \frac{1.33}{1.38} * 1.66 = 1.60 \quad \text{(B5)}$$

As for the β value for =CH-, this parameter was estimated through back calculation using the FFV of a well-studied polymer, polybutadiene [3]. This calculation is outlined below.

$$FFV_{PB} = 0.157 = \frac{(2*\beta_{w,=CH}*V_{w,=CH})+(2*\beta_{w,CH2}*V_{w,CH2})-1.3*[(2*V_{w,=CH})+(2*V_{w,CH2})]}{(2*\beta_{w,=CH}*V_{w,=CH})+(2*\beta_{w,CH2}*V_{w,CH2})} \quad \text{(B6)}$$

$$0.157 = \frac{(2*\beta_{w,=CH}*8.47)+(2*1.33*10.23)-1.3*[(2*8.47)+(2*10.23)]}{(2*\beta_{w,=CH}*8.47)+(2*1.33*10.23)} \quad \text{(B7)}$$

$$\beta_{w,=CH} = 1.799 \quad \text{(B8)}$$

Now that all functional groups in the pNBFn structure are accounted for, the FFV values of the polymers in this study were calculated and are summarized in **Table B2**. As an example, for pNBF4, the calculation is outlined below. This result closely matches FFV calculations performed by others [4].

$$V_{w,pNBF4} = (2 * V_{w,CH2}) + (3 * V_{w,CH}) + (2 * V_{w,=CH}) + (V_{w,decrament}) + (3 * V_{w,CF2}) + V_{w,CF3}$$

$$V_{w,pNBF4} = (2 * 10.23) + (3 * 6.78) + (2 * 8.47) + (-1.14) + (3 * 15.94) + 21.3 = 125.72 \frac{cm^3}{mole} \quad \text{(B9)}$$

$$V_{sp,pNBF4} = (2 * \beta_{CH2} * V_{w,CH2}) + (3 * \beta_{CH} * V_{w,CH}) + (2 * \beta_{=CH} * V_{w,=CH}) + (V_{w,decrament}) + (3 * \beta_{CF2} * V_{w,CF2}) + \beta_{CF3} * V_{w,CF3} \quad \text{(B10)}$$

$$V_{sp,pNBF4} = (2 * 1.33 * 10.23) + (3 * 1.3 * 6.78) + (2 * 1.799 * 8.47) + (-1.14) + (3 * 1.60 * 15.94) + 1.66 * 21.3 = 197.73 \frac{cm^3}{mole} \quad \text{(B11)}$$

$$FFV_{pNBF4} = \frac{V_{sp}-1.3*V_w}{V_{sp}} = \frac{197.73-1.3*(125.72)}{197.73} = 0.173 \quad \text{(B12)}$$

Table B2: Bondi FFV values calculated for pNB, pNBF4, pNBF6, pNBF8, and pNBF10 using the parameters summarized in Table B1

Polymer	***Bondi FFV***
pNB	0.111
pNBF4	0.173
pNBF6	0.183
pNBF8	0.189
pNBF10	0.193

C. Contact Angle Goniometry on Gold and Polyacrylonitrile (PAN) Substrates:

Contact angle measurements for pNB and pNBFn on gold are reported in **Figure 7** of the manuscript. The measurements were taken on gold to allow comparison to previous studies conducted on these polymers [5]. **Table C1** shows that the contact angles on films on PAN are within range of those taken on gold for both scROMP and SI-ROMP manufacturing techniques.

Table C1: Advancing contact angle measurements of hexadecane and water for pNBF4 and pNBF6 surfaces on PAN and gold substrates.

Sample	Hexadecane	Water	Source
pNBF4 on PAN	61	111	This work
pNBF4 on Gold	60	123	This work
pNBF4 on Gold	61	110	[5]
pNBF6 on PAN	68	118	This work
pNBF6 on Gold	66	124	This work
pNBF6 on Gold	67	116	[5]

D. Pervaporation Experiment Process Flow Diagram:

For the pervaporation experiments conducted in this manuscript, the setup depicted in **Scheme D1** was utilized.

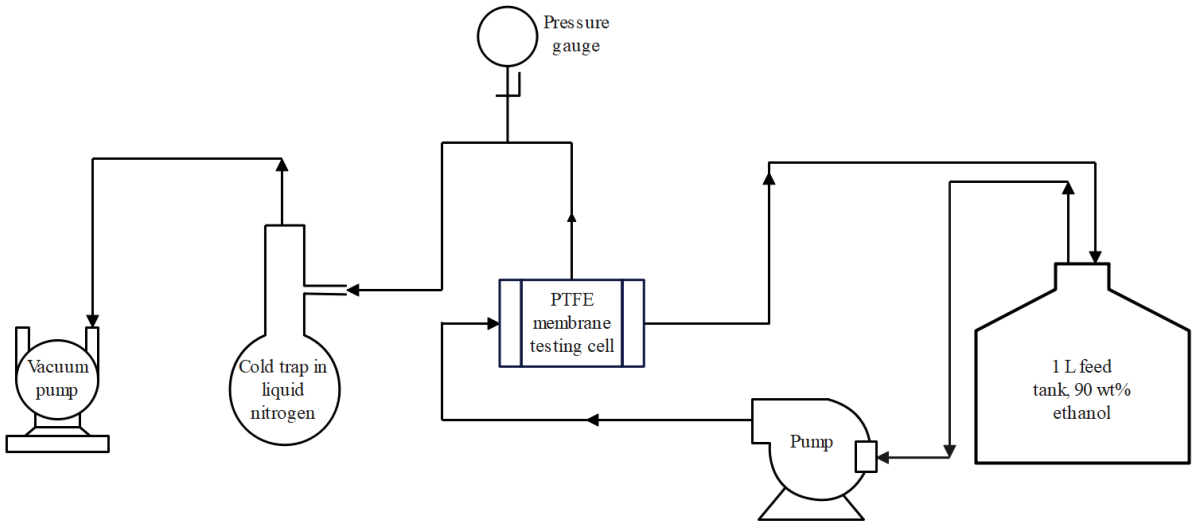

Scheme D1: Schematic diagram of the membrane pervaporation setup. From right to left, 90 wt% ethanol flows from 1 L feed tank through the front of the membrane testing cell using a pump. The permeate stream is collected from the back of the testing cell into a liquid nitrogen-cooled cold trap under vacuum, and the retentate is recycled to the feed tank.

E. SEM and EDS Images:

Figure E1 shows a lower magnification SEM image of a pNBF8 film that was deposited at a monomer spin speed of 3,000 rpm. This image shows the polyester backing, no separation of the pNBF8 film from the PAN, and a pNBF8 thickness of generally < 15 μm that is consistent with those of the pNBF8 membranes tested for pervaporation.

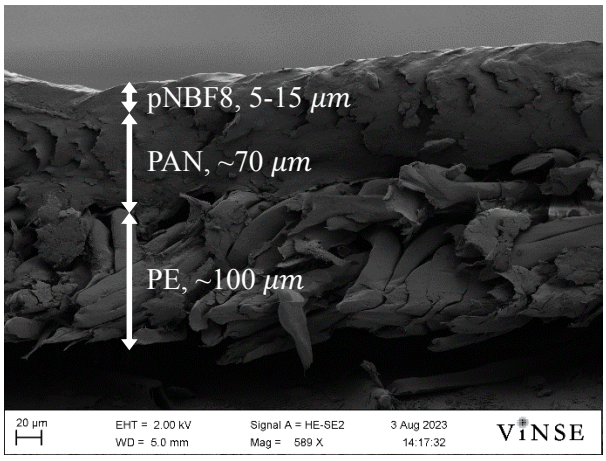

Figure E1: SEM image of a pNBF8 film on a PAN-coated polyester backing support.

Figure E2 shows the electron image from the EDS images shown as Figures 4b, c, and d in the manuscript.

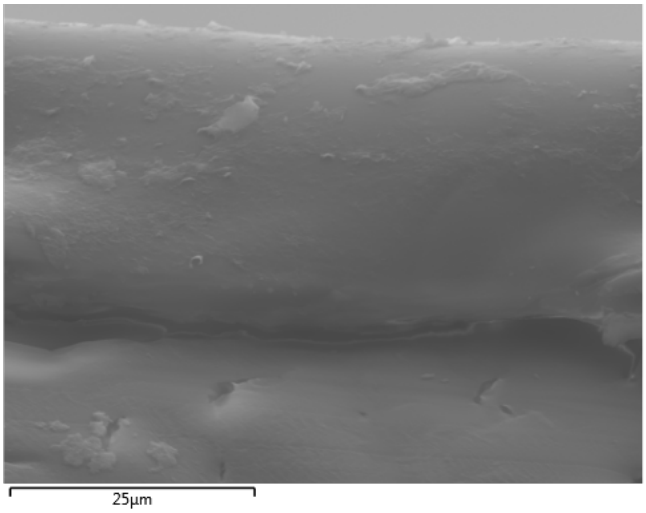

Figure E2: Electron image acquired during EDS and subsequently used for elemental mapping in **Figures 4b, c,** and **d.**

F. Membrane Stability:

While the stability of pNBFn membranes was shown through limited swelling at room temperature and extensive operating times (>40 h), the integrity of the polymer film was also confirmed using ATR-FTIR spectroscopy. First, pNB and pNBFn films were grown on a 30 kDa molecular weight cutoff PAN support using scROMP. Then, the films were characterized using IR spectroscopy before and after flowing 90 wt% ethanol across them for 6 h at 60 °C, which replicates the typical film exposure during a pervaporation experiment. The post-IR scan of the film was used to determine if the exposure to 90/10 (w/w) ethanol/water at elevated temperature altered the absorbance of any molecular groups in the polymer film. **Figure F1** shows IR spectra for each polymer before and after the 6 h exposure. The pNBFn films show no significant decrease in the absorbance of their fluorocarbon peaks and no meaningful increases in the presence of nitrile or ester functionalities from the underlying PAN support. This lack of change indicates that these polymers attenuate the PAN substrate at an indistinguishable level as before the solvent exposure. Conversely, the pNB film exhibits a large decrease in the absorbance of its vinylene (970 cm^{-1}) peak and dramatic increases in nitrile and ester stretching. The pNB vinylene (HC=CH) 970 cm^{-1} absorbance decreased by nearly one half (~0.45 to ~0.24) while the nitrile (2242 cm^{-1}) nearly doubled (~0.04 to ~0.07), indicating reduced coverage of the underlying PAN after solvent exposure. Evidence of oxidation of the pNB backbone is apparent by the presence of increased O-H stretching centered at about 3400 cm^{-1} and carbonyl stretching at 1760 cm^{-1}. An instability of pNB films has been previously reported by us and others attributed to oxidation of the unsaturated backbone [5,6].

This chemical instability is not observed for the pNBFn system, likely due to the perfluoro moiety diluting the concentration of the olefin functionality within the film, which offers greater kinetic stability [5]. Furthermore, the long chains can serve as effective shields preventing access to the backbone of the molecule for reaction and thus dissuading oxidation. Therefore, the pNBFn films remain intact and provide the same level, or near the same level of coverage of the PAN support after exposure to the 90/10 wt% ethanol/water mixture while the pNB film exhibits clear signs of chemical instability.

The performance of pNBF8 membranes is stable upon multiple pervaporation tests of the same membrane. For example, we tested a pNBF8 membrane repeatedly for four days at 60 °C, let it sit in the feed solution at room temperature for two additional days, and then tested again at 60 °C on the seventh day. The results (see **Table F1**) show that the selectivity (α = 170 - 220) and separation factor (β = 85 – 110) remain high during the entire week-long study. The total flux decreased by ~25% after the first day and another ~20% after the third day but was stable over the latter half of the week. We note that the consistent separation performance along with the absence of a dramatic increase in flux indicates that the membrane exhibits good stability over the week-long exposure to the feed solution and pervaporation experiments.

Table F1: Repeated pervaporation testing of the same pNBF8 membrane at 60°C in 90/10 (wt) ethanol/water. On days 5-6, the membrane was stored in the feed solution at 22°C.

Day	$J\left(\frac{g}{m^2 h}\right)$	$\frac{P^G_{H_2O}}{l}$ (GPU)	$\frac{P^G_{EtOH}}{l}$ (GPU)	α	β	Weight Percent EtOH
1	85	660	3	220	110	7.5
2	63	490	2	200	100	8.0
3	66	520	2	220	110	7.5
4	52	440	2	200	100	8.0
7	51	390	2	170	85	9.5

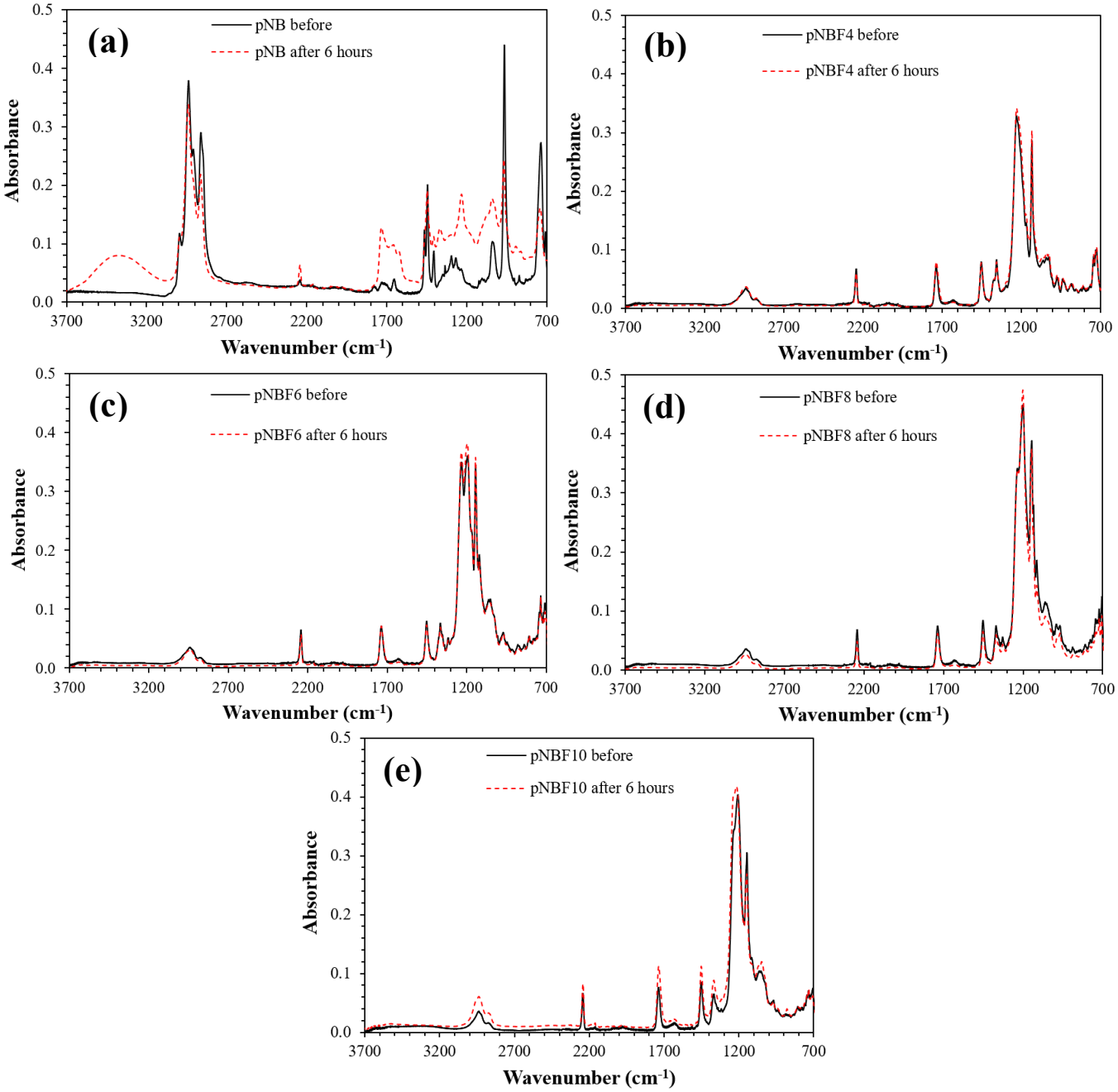

Figure F1: ATR-FTIR spectra of (a) pNB, (b) pNBF4, (c) pNBF6, (d) pNBF8, and (e) pNBF10 films before and after exposure to a flowing 90 wt% ethanol solution at 60 °C for 6 h. The spectra confirm that the pNBFn polymer films (b-e) provide the same, or near the same level of coverage of the underlying PAN support after testing while pNB (a) is prone to oxidation of its unsaturated backbone.

G. Differential Scanning Calorimetry (DSC) Curves:

The glass transition temperatures (T_g) of pNB and pNBFn were measured from the scans in **Figure G1**. T_g was determined using the glass transition tool in the TRIOS DSC 25 software and reported in **Table 2** of the manuscript.

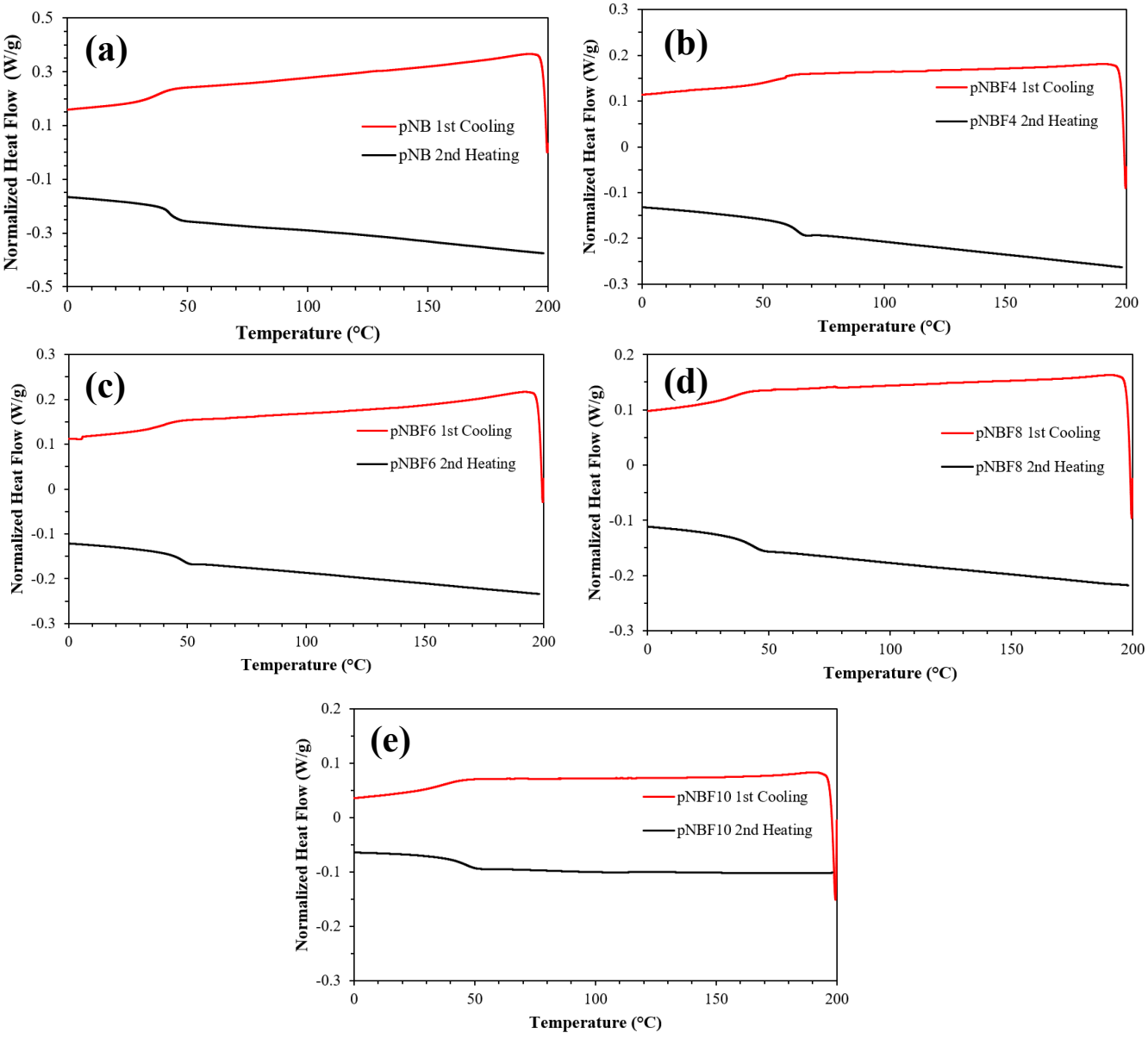

Figure G1: DSC curves of (a) pNB, (b) pNBF4, (c) pNBF6, (d) pNBF8, and (e) pNBF10.

H. Comparison of pNBFn Membrane Performance in Ethanol Dehydration:

Figure H1 compares the performance of pNBFn membranes reported here with leading hydrophilic (PVA, chitosan, cellulose, and alginate) and hydrophobic membranes for the dehydration of ethanol by membrane pervaporation. The pNBFn membranes are among the better performing hydrophobic membranes but trail the top-performing hydrophilic ones.

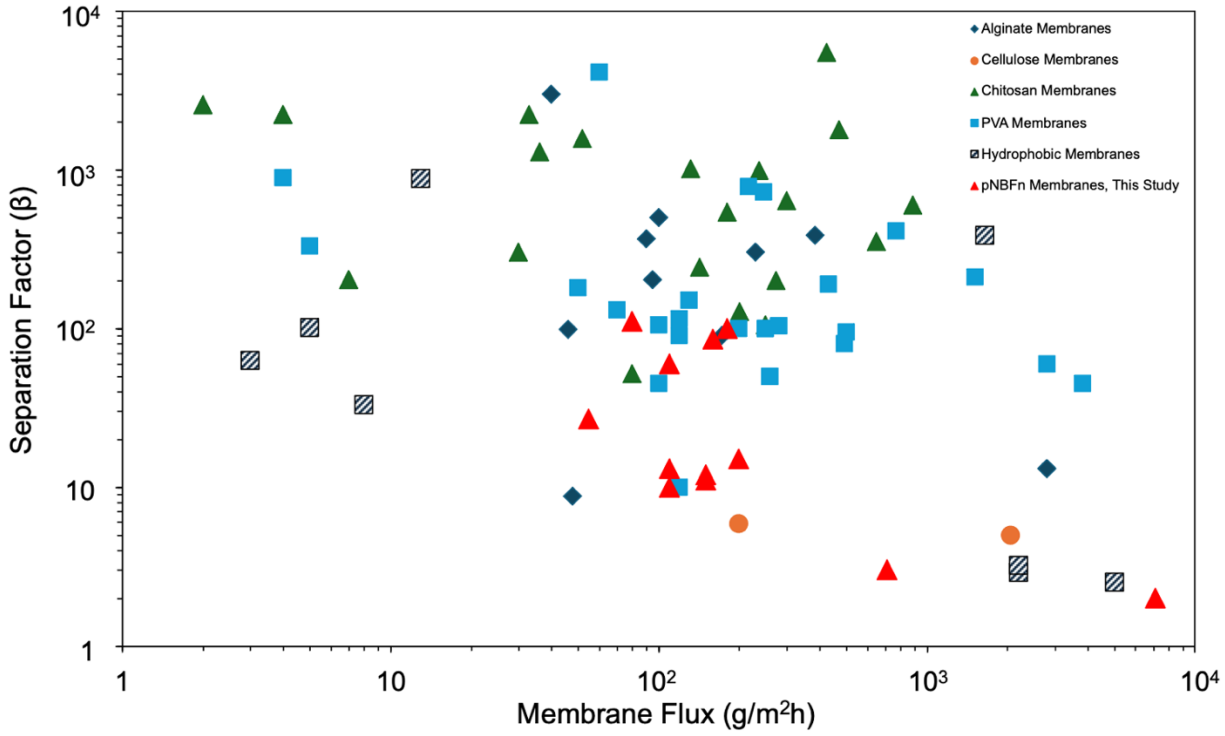

Figure H1: Comparison of pNBFn membranes (red) to other hydrophilic and hydrophobic membranes as reported by Bolto et al.[7] and Chapman et al.[8].

I. Molecular Dynamics Simulation:

I1. Protocols for generating bulk polymers and thin films:

Bulk Polymers

Five separate monodisperse bulk polymer systems corresponding to pNBFn, n = 0, 4, 6, 8 and 10 were created by randomly packing energy minimized polymer chains into a cubic simulation box (see **Figure I1.1a**) corresponding to a gas phase density of 40 kg/m^3 (see **Table I1.1** for system specifications) using mbuild [9]. A minimum-distance requirement of 2 Å between atoms of different chains was set to avoid significant steric overlaps. The system was then equilibrated in the NVT ensemble under periodic boundary conditions at 15 K for 1 ns to prevent the polymer chains from collapsing. Next, the 21-step equilibration protocol established by Abbott et al. [10] in which a bulk polymer system is transformed from an initial gaseous phase to a condensed phase was followed. The polymer system undergoes gradual compression and expansion, as well as sequential heating and cooling cycles, to achieve a condensed phase density corresponding to the desired temperature, T_{final} and pressure, P_{final}. Here, the T_{final} and P_{final} were set to 300 K and 1 atm, respectively. During the compression and heating steps, the maximum pressure and temperature used were 50000 bar and 400 K, respectively. **Figure I1.1c** shows the instantaneous density of a representative sample polymer as it undergoes different stages of the protocol. The final configuration after the 21-step equilibration protocol is shown in **Figure I1.1b.** Using the annealed configuration at 300 K NPT simulations were carried out for 10 ns. The box size of the polymer systems in any given dimension ranged between (6.7 -7.2 nm).

Table I1.1. Specifications of polymer models

System	# Repeat units /chain	# Monomer chains	# Atoms
pNB	30	60	30960

pNBF4	30	32	28032
pNBF6	30	27	28512
pNBF8	30	23	28428
pNBF10	30	21	29736

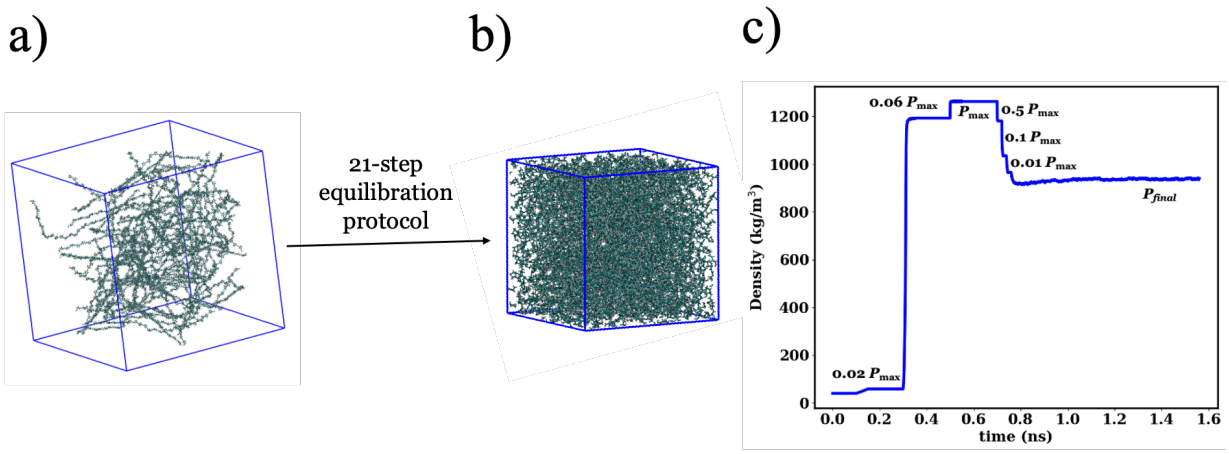

Figure I1.1: Representative polymer system (pNB) in the gas phase (a) and after the 21-step equilibration protocol (b) and evolution of bulk polymer (pNB) density throughout the 21-step equilibration protocol (c)

Polymer Films

Free standing thin films of pNBFn polymers of nano-scale dimensions were constructed following a procedure similar to Li et al. [11]. The bulk polymer system (**Figure I1.2a**) was replicated twice in the z-dimension and a continuous film generated through the manipulation of periodic boundary conditions. The z-dimension was then unwrapped and 5 nm of vacuum was added on both sides (**Figure I1.2b)**. Structureless Lennard Jones (LJ) walls (σ = 0.355 nm, ε = 0.318 kJ/mol) were then placed on both sides of the z-dimension (**Figure I1.2c)** and the polymer system subject to the same 21-step equilibration

protocol as for the bulk polymer systems. During this protocol, 2D periodic boundary conditions and semi-isotropic pressure coupling were used. The values of T_{final}, P_{final}, P_{max}, T_{max} were the same as those used for equilibrating the bulk polymer system. Finally, the walls were removed, and a vacuum layer was again added on both sides of the film (**Figure I1.2d**). To allow sufficient time for configurational re-arrangement of chains on the surface after removal of the walls, the films were then simulated in the NVT ensemble for a further 600 ns.

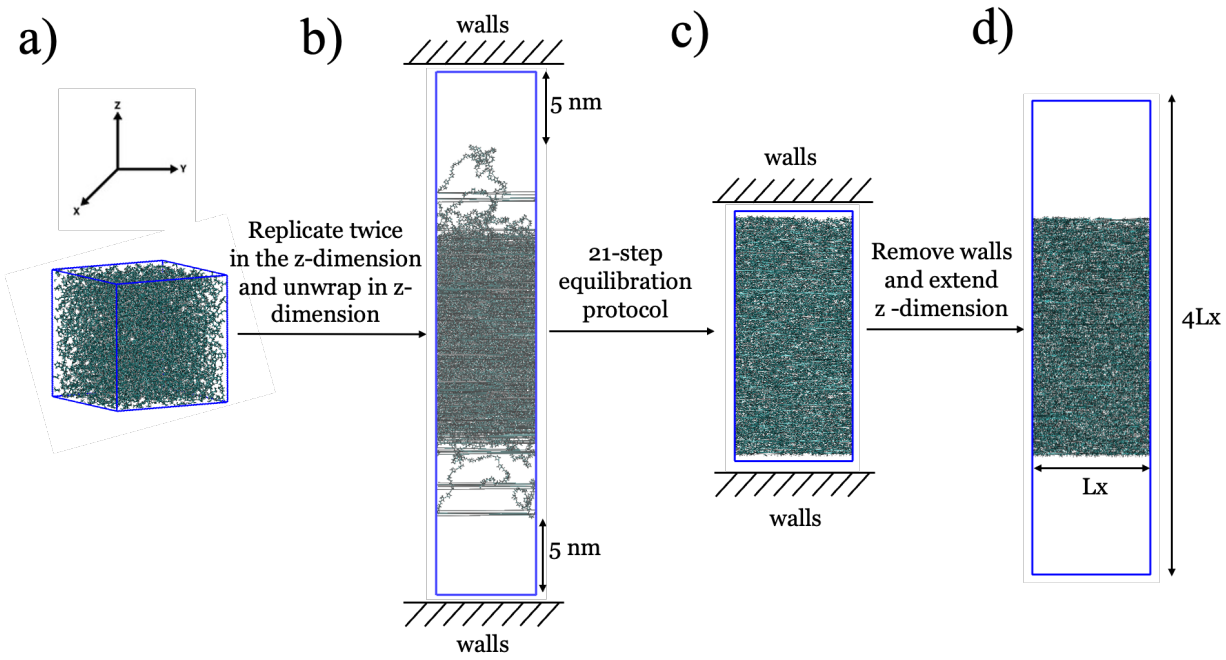

Figure I1.2: Steps illustrating the creation of a free-standing polymer film (representative system, pNB). (a) bulk polymer system (b) bulk polymer system after replication in the z-dimension (c) configuration at the end of 21-step step equilibration protocol (d) free standing film.

I2. General simulation and analysis details:

In all simulations, a non-bonded interaction cut-off of 1.2 nm was used and long-range corrections applied to both the pressure and energy. Long-range electrostatics were considered using PME [12,13] with a grid spacing of 0.4 nm and an interpolation order of 4. All bonds involving hydrogen atoms were kept rigid using the linear constraint solver, LINCS [14]. Temperature control was achieved through the use of velocity re-scaling with a stochastic component [15] and a time constant of 1 ps. The pressure was regulated using the cell-rescaling algorithm with a stochastic term [16]. For bulk polymer simulations, the time constant and compressibility for the re-scaling algorithm used were 6 ps and 4.5 x 10^{-5} bar^{-1}, respectively. For thin film simulations, the same time constant was used but a slightly lower value for the compressibility, 1 x 10^{-5} bar^{-1} was used. A timestep of 1 fs was used for the 21-step equilibration protocol (including the initial NVT equilibration) and for all other simulations, a timestep of 2 fs was used. To improve statistical uncertainties in simulated properties, three independent replicas of the bulk polymer and thin film systems were simulated. The GROMACS files and python codes necessary to reproduce the simulation results can be downloaded from https://github.com/PTC-CMC/PNBFN_signac.

Details of properties calculated, the corresponding analysis tool used, the total time for which the simulations were run, and the length of the trajectory used for calculation of properties are summarized in the following table. Values reported in the table are for one polymer replica.

Property	**Analysis tool**	**Total trajectory length**	**Trajectory used for data acquisition and calculations (# of frames)**

Radial distribution function at 300 K	GROMACS utility tool (gmx rdf)	20 ns	Last 5 ns (26 frames)
Dihedral distributions at 300 K	GROMACS utility tool (gmx angle)	20 ns	Last 5 ns (26 frames)
Density of bulk polymers at 300 K	GROMACS utility tool (gmx energy)	20 ns	Last 5 ns (26 frames)
Radius of gyration of bulk polymers	GROMACS utility tool (gmx polystat)	600 ns	Last 5 ns (26 frames)
Free volume properties of the bulk polymer	Poreblazer	100 ns	100 ns (3 frames, sampled at 0, 50 and 100 ns)
Interfacial density profile of thin films	GROMACS utility tool (gmx energy)	600 ns	Last 20 ns (41 frames)
Surface composition and orientation of chains in polymer films	MDanalysis	600 ns	Last 100 ns (201 frames)
Radius of gyration of thin films	GROMACS utility tool (gmx polystat)	600 ns	Last 20 ns (41 frames)

I.3. Equilibration of Bulk Polymers and Thin Films:

Well equilibrated polymer simulations are necessary to ensure that the properties evaluated with the chosen force field model are valid [17]. For this purpose, the radius of gyration of chains, *Rg*, in the bulk polymer and in thin films at 300 K was monitored over a period time. The *Rg* of a polymer chain was calculated according to,

$$Rg = \frac{1}{N}\left(\sum_{i=1}^{N}\left(r_i(t) - r_{cm}(t)\right)^2\right)$$

where, *N,* $r_i(t)$ and $r_{cm}(t)$ are the number of atoms, position vector of atoms at any given time, t, and the mean position vector of the atoms at any given time, t, respectively. The calculated values of *Rg* for the bulk and thin films are shown in **Figure I.3.1** and **Figure I.3.2**. As can be seen, the radius of gyration does not drift with time, suggesting that the simulations of the bulk and thin films are well equilibrated.

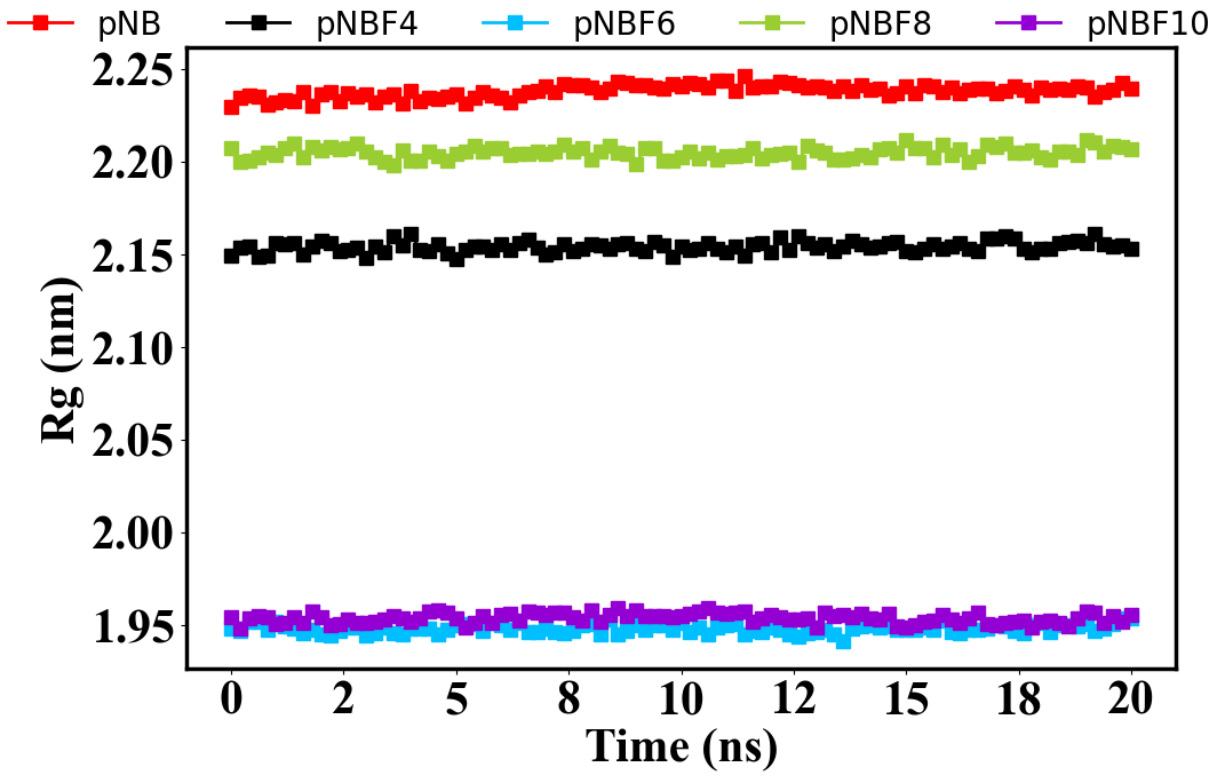

Figure I.3.1: Radius of gyration of chains, *Rg* of bulk polymers at 300 K. Each curve represents data for one replica of the polymer. Uncertainties not shown for clarity

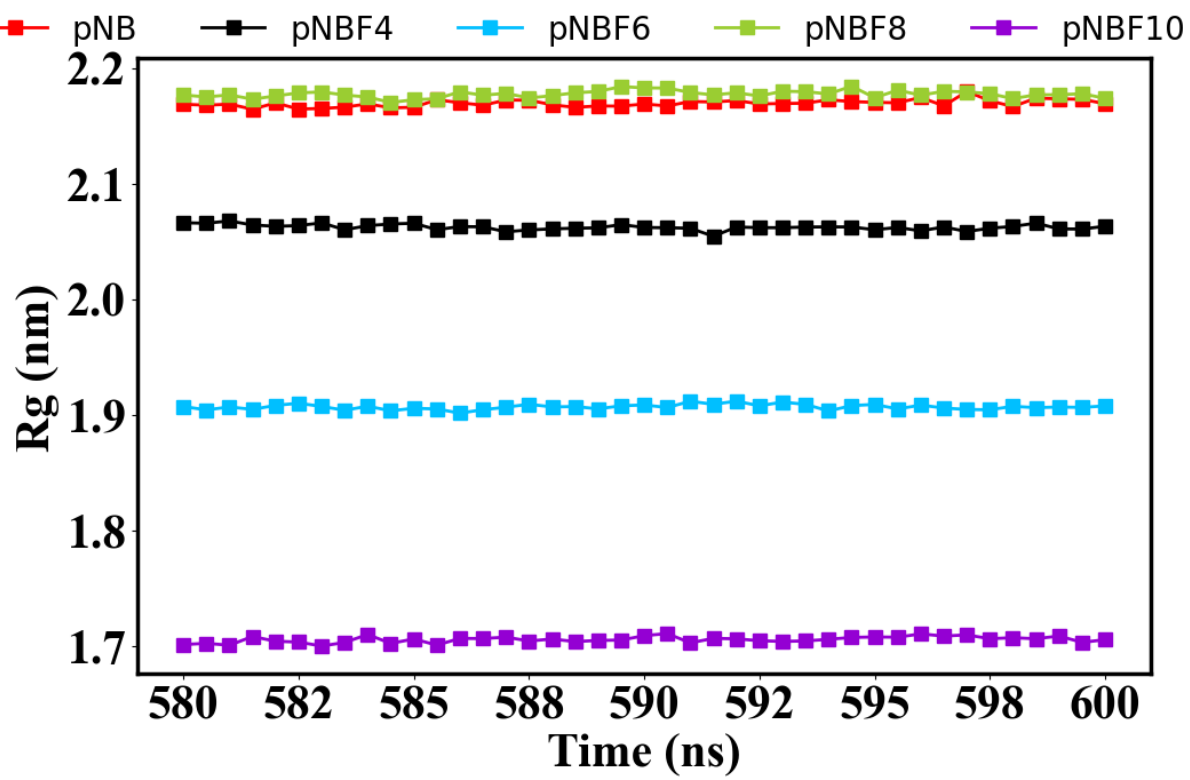

Figure I.3.2: Radius of gyration of chains, *Rg* of bulk polymers at 300 K. Data from last 20 ns of 600 ns trajectory is shown. Each curve represents data for one replica of the polymer. Uncertainties not shown for clarity

Nano-scale thin films generated from atomistic simulations can suffer from instabilities due to capillary waves or other thermal fluctuations [18]. Such instabilities can often be diagnosed by inspecting the film density profiles. In the present case, the density profiles of the films showed no aberrations for the timescale (>100 ns) and for the temperature of interest (300 K), indicating that the films are stable. In all cases, a central region corresponding to homogeneous bulk fluid characterized by a flat density profile was apparent (see **Figure I.3.3**). Moreover, the thickness of the films (the thickness was calculated as the distance between the maximum and the minimum z-coordinate of the atoms) ranged between 14-16 nm, which is significantly higher than the radius of gyration (maximum value of the radius of gyration in the pNBFn polymer films does not exceed 2.6 nm). These observations also imply that finite size effects will have negligible impact on film properties [19].

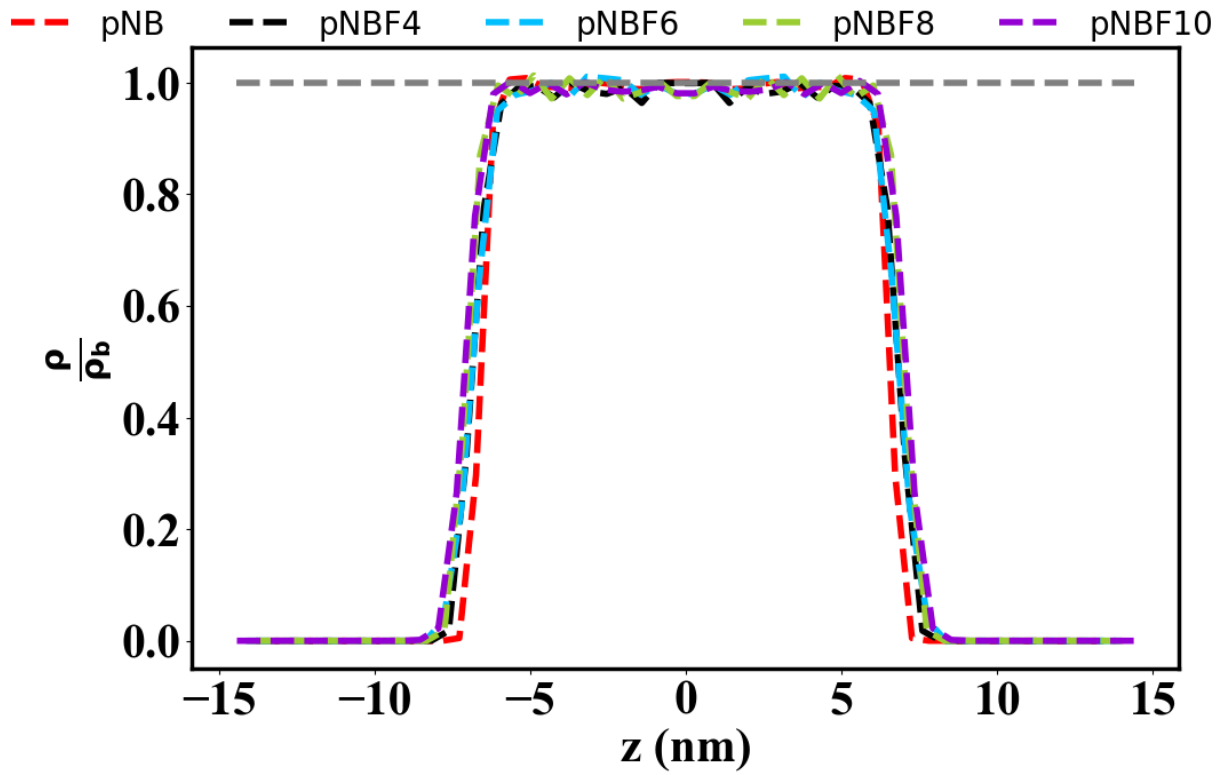

Figure I.3.3: Normalized density profiles (time averaged) of polymer films at 300 K. Each curve represents data from one replica. ρ denotes the density of the film and ρ_b denotes the average density of the bulk polymer (see Table 1 in the main text).

I.4. Calculation of surface composition and orientation of side chain vectors in thin films:

The orientation of side-chain vectors in the pNBFn films is characterized based on $\cos\theta$, defined by

$$\cos\theta = \frac{\vec{u}.\vec{n}}{|\vec{u}||\vec{n}|}$$

where, $\vec{u}$ is the vector joining the two ends of the carbon atoms of the perfluoro chains and $\vec{n}$ is the surface normal vector. Based on centre of gravity of the atoms, the central region of the film was divided into two blocks each of 2 nm thickness (**see Figure I.4.1,** the central blocks are shown in red). For the upper block and lower block, $\vec{n}$ was taken to be [0,0,1] and [0,0,-1], respectively. A side chain was determined to be in a block, if the end carbon atom of the side chain was in the block. All chain vectors in

the two blocks were considered and configurations from the last 20 ns of 600 ns trajectory were used in the calculation of $\cos\theta$. Similar calculations were performed to analyze the orientation of chain vectors in the interface region (interface region was taken to be 1.8 nm from the polymer/air interface). The distributions of θ were then calculated and further smoothed using the KDE functionality in the statsmodel python package.

The surface excess composition is calculated according to the following equation,

$$\text{Surface excess}=\frac{X_{surface}}{X_{center}}-1$$

where $X_{surface}$ is the number fraction of a specific functional group (CF3, CF2 or CH2) in the interface region and X_{center} is the number fraction of the functional group in the central region of the film. Both top and bottom interfacial regions were considered in the calculation of $X_{surface}$. The thickness of the central region for calculating X_{center} was considered to be twice that of the interface region (3.6 nm).

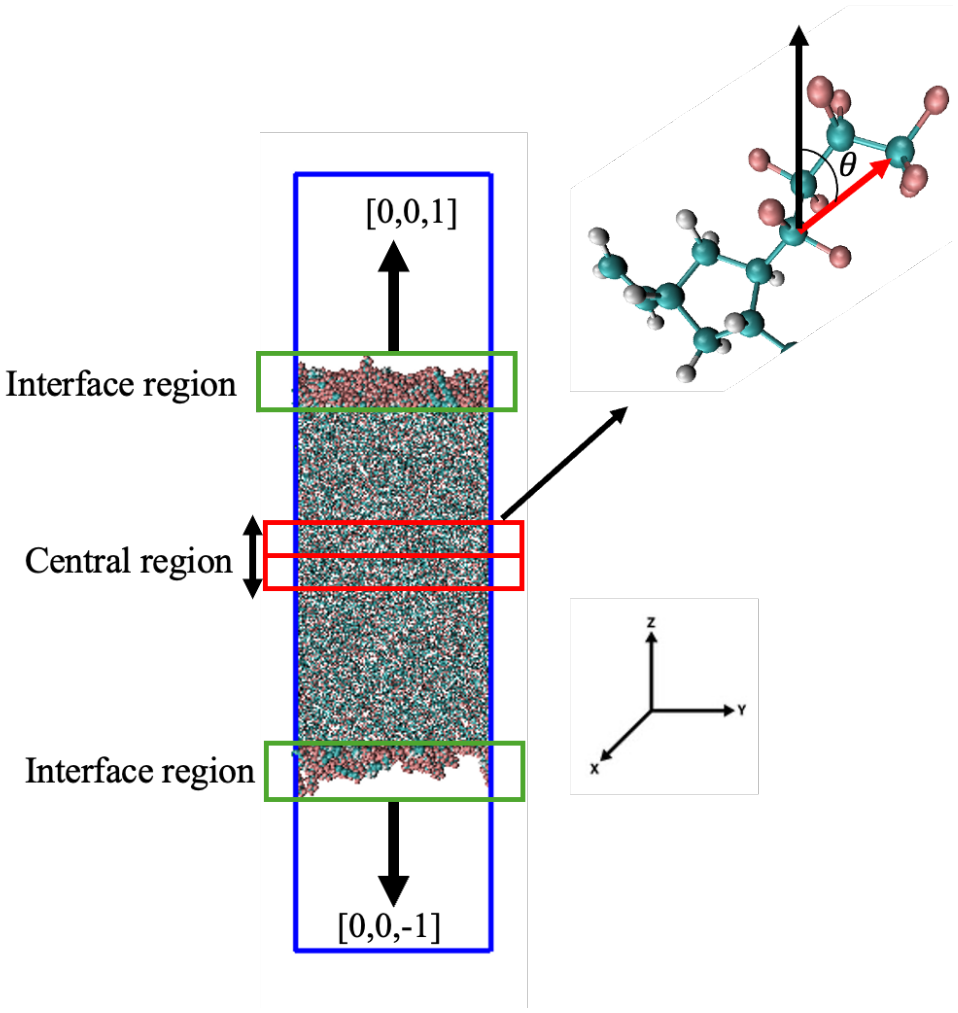

Figure I.4.1: Simulation snapshot illustrating the central region and the interface region in the simulation cell (carbon atoms are represented by cyan spheres, hydrogen atoms by white and fluorine by purple, two central blocks, each are shown in red, surface blocks are shown in green) from which the angle θ between the vector joining the two ends of the carbon atoms of the perfluoro chain (denoted by red arrow) and the normal to the x-y plane (black arrow) is determined.

I.5. Calculation of free volume properties:

The Poreblazer tool [20] was used to calculate the free volume properties and pore size distribution of the polymers studied. The free volume properties were sampled from three configurations at time instants of 0, 50 and 100 ns for three replica simulations of each system studied (i.e., a total of 9 configurations were

used each polymer system). By default, Poreblazer uses the UFF (universal force field) to assign Lennard Jones parameter (σ) to the atoms. This process was altered in the present case to be consistent with the OPLS-AA force field used in the simulations. The σ of carbon, hydrogen and fluorine (species that constitute pNBFn polymers) used were 3.5, 2.45 and 2.95 Å, respectively. Further, the search for the largest cavity diameter was restricted to 9 Å. The PSDs reported in this work represent the total PSD and not the network-accessible PSD.

J. Additional analysis on the local structure:

It is known that side chain substitution can alter the conformational flexibility of five membered rings [21] and can therefore affect molecular packing. The conformational flexibility is analyzed based on the distributions of torsion angles involving the carbon atoms in the cyclopentylene rings of pNB and pNBFn polymers and are shown in **Figure J1a**. It is clear that cyclopentylene rings adopt planar configurations (non-trivial values for $\theta = 0$), however these configurations are less preferred over puckered configurations (two peaks) to minimize eclipsing strain (eclipsing strain arises when hydrogens are positioned in a perfect planar conformation) [22]. This is further confirmed by the distribution of the angles in the cyclopentylene rings (**Figure J1b**). The average value of θ is 105^0 which is less than the angle in the rings if they were to be planar (angles in a pentagon is 108^0). Distributions in **Figure J1** further show no significant sensitivity to chain length suggesting that torsional strain is not influenced by chain length.

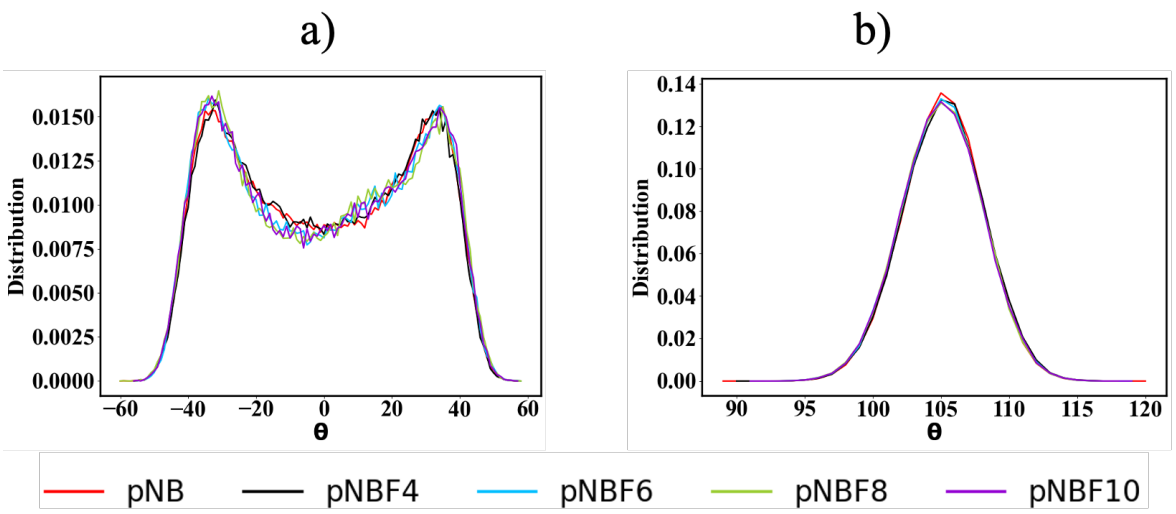

Figure J1: (a) Distributions of the torsion angles formed by carbon atoms in the cyclopentylene rings.

References:

[1] Bondi A. van der Waals Volumes and Radii. J Phys Chem 1964;68:441–51. https://doi.org/10.1021/j100785a001.

[2] Park JY, Paul DR. Correlation and prediction of gas permeability in glassy polymer membrane materials via a modified free volume based group contribution method. Journal of Membrane Science 1997;125:23–39. https://doi.org/10.1016/S0376-7388(96)00061-0.

[3] Mazo M, Balabaev N, Alentiev A, Yampolskii Y. Molecular dynamics simulation of nanostructure of high free volume polymers with $SiMe_3$ side groups. Macromolecules 2018;51:1398–408. https://doi.org/10.1021/acs.macromol.7b02470.

[4] Adzhieva OA, Nikiforov RYu, Gringolts ML, Belov NA, Filatova MP, Denisova YuI, et al. Synthesis and gas separation properties of metathesis poly(5-perfluorobutyl-2-norbornene). Polym Sci Ser A 2022;64:424–33. https://doi.org/10.1134/S0965545X22700262.

[5] Faulkner CJ, Fischer RE, Jennings GK. Surface-Initiated polymerization of 5-(perfluoro-n-alkyl)norbornenes from gold substrates. Macromolecules 2010;43:1203–9. https://doi.org/10.1021/ma902249m.

[6] Seehof N, Grutke S, Risse W. Selective reaction with exo-isomers in ring-opening olefin metathesis polymerization (ROMP) of fluoroalkyl-substituted norbornene derivatives. Macromolecules 1993;26:695–700. https://doi.org/10.1021/ma00056a021.

[7] Bolto B, Hoang M, Xie Z. A review of membrane selection for the dehydration of aqueous ethanol by pervaporation. Chemical Engineering and Processing: Process Intensification 2011;50:227–35. https://doi.org/10.1016/j.cep.2011.01.003.

[8] Chapman PD, Oliveira T, Livingston AG, Li K. Membranes for the dehydration of solvents by pervaporation. Journal of Membrane Science 2008;318:5–37. https://doi.org/10.1016/j.memsci.2008.02.061.

[9] Klein C, Sallai J, Jones TJ, Iacovella CR, McCabe C, Cummings PT. A Hierarchical, Component based approach to screening properties of soft matter. In: Snurr RQ, Adjiman CS, Kofke DA, editors. Foundations of Molecular Modeling and Simulation: Select Papers from FOMMS 2015, Singapore: Springer; 2016, p. 79–92. https://doi.org/10.1007/978-981-10-1128-3_5.

[10] Abbott LJ, Hart KE, Colina CM. Polymatic: a generalized simulated polymerization algorithm for amorphous polymers. Theor Chem Acc 2013;132:1334. https://doi.org/10.1007/s00214-013-1334-z.
[11] Li Z, Yuan F, Fichthorn KA, Milner ST, Larson RG. Molecular view of polymer/water interfaces in latex paint. Macromolecules 2014;47:6441–52. https://doi.org/10.1021/ma500866f.
[12] Darden T, York D, Pedersen L. Particle mesh Ewald: An N·log(N) method for Ewald sums in large systems. The Journal of Chemical Physics 1993;98:10089–92. https://doi.org/10.1063/1.464397.
[13] Essmann U, Perera L, Berkowitz ML, Darden T, Lee H, Pedersen LG. A smooth particle mesh Ewald method. The Journal of Chemical Physics 1995;103:8577–93. https://doi.org/10.1063/1.470117.
[14] Hess B. P-LINCS: a parallel linear constraint solver for molecular simulation. J Chem Theory Comput 2008;4:116–22. https://doi.org/10.1021/ct700200b.
[15] Bussi G, Donadio D, Parrinello M. Canonical sampling through velocity rescaling. The Journal of Chemical Physics 2007;126:014101. https://doi.org/10.1063/1.2408420.
[16] Bernetti M, Bussi G. Pressure control using stochastic cell rescaling. The Journal of Chemical Physics 2020;153:114107. https://doi.org/10.1063/5.0020514.
[17] Lyulin SV, Gurtovenko AA, Larin SV, Nazarychev VM, Lyulin AV. Microsecond atomic-scale molecular dynamics simulations of polyimides. Macromolecules 2013;46:6357–63. https://doi.org/10.1021/ma4011632.
[18] González-Mijangos JA, Lima E, Guerra-González R, Ramírez-Zavaleta FI, Rivera JL. Critical thickness of free-standing nanothin films made of melted polyethylene chains via molecular dynamics. Polymers 2021;13:3515. https://doi.org/10.3390/polym13203515.
[19] Neyertz S, Brown D. An optimized fully-atomistic procedure to generate glassy polymer films for molecular dynamics simulations. Computational Materials Science 2020;174:109499. https://doi.org/10.1016/j.commatsci.2019.109499.
[20] Sarkisov L, Bueno-Perez R, Sutharson M, Fairen-Jimenez D. Materials informatics with PoreBlazer v4.0 and the CSD MOF database. Chem Mater 2020;32:9849–67. https://doi.org/10.1021/acs.chemmater.0c03575.
[21] Stortz CA, Sarotti AM. Exhaustive exploration of the conformational landscape of mono- and disubstituted five-membered rings by DFT and MP2 calculations. RSC Adv 2019;9:24134–45. https://doi.org/10.1039/C9RA03524A.
[22] Karnik AV, Hasan M. Chapter 8 - Conformations of cyclic, fused and bridged ring molecules. In: Karnik AV, Hasan M, editors. Stereochemistry, Elsevier; 2021, p. 273–375. https://doi.org/10.1016/B978-0-12-821062-8.00010-7.